Adaptive Multi-class Segmentation Model of Aggregate Image Based on Improved Sparrow Search Algorithm

Mengfei Wang[1*], Weixing Wang[1*], Sheng Feng[2] and Limin Li[3*]
[1] School of Information, Chang'an University
Xi'an, Shaanxi, China
[e-mail: m.f.wang@foxmail.com and wxwang@chd.edu.cn]
[2] Computer Science and Engineering, Shaoxing University
Shaoxing, Zhejiang, China
[e-mail: fengsheng_13@aliyun.com]
[3] School of Electrical and Electronic Engineering, Wenzhou University
Wenzhou, Zhejiang, China
[e-mail: lilimin@wzu.edu.cn]
[*]Corresponding author: Weixing Wang and Limim Li

Abstract

Aggregates play the skeleton and supporting role in the construction field, high-precision measurement and high-efficiency analysis of aggregates are frequently employed to evaluate the project quality. Aiming at the unbalanced operation time and segmentation accuracy for multi-class segmentation algorithms of aggregate images, a Chaotic Sparrow Search Algorithm (CSSA) is put forward to optimize it. In this algorithm, the chaotic map is combined with the sinusoidal dynamic weight and the elite mutation strategies; and it is firstly proposed to promote the SSA's optimization accuracy and stability without reducing the SSA's speed. The CSSA is utilized to optimize the popular multi-class segmentation algorithm-Multiple Entropy Thresholding (MET). By taking three METs as objective functions, i.e., Kapur Entropy, Minimum-cross Entropy and Renyi Entropy, the CSSA is implemented to quickly and automatically calculate the extreme value of the function and get the corresponding correct thresholds. The image adaptive multi-class segmentation model is called CSSA-MET. In order to comprehensively evaluate it, a new parameter I based on the segmentation accuracy and processing speed is constructed. The results reveal that the CSSA outperforms the other seven methods of optimization performance, as well as the quality evaluation of aggregate images segmented by the CSSA-MET, and the speed and accuracy are balanced. In particular, the highest I value can be obtained when the CSSA is applied to optimize the Renyi Entropy, which indicates that this combination is more suitable for segmenting the aggregate images.

Keywords: Aggregate particle, Chaotic map, Entropy, Image multi-class segmentation, Optimization, Sparrow search algorithm

1. Introduction

$\mathbf{A}$ggregate is the main raw material of concrete, and the geometric characteristics of aggregates determine the mechanical properties of concrete [1]. Affected by aggregate source, rock type, crushing method and grinding degree, it is difficult to accurately and quickly measure the rough surface texture, edge shape, particle size and other characteristics of aggregate [2]. Image processing techniques can be utilized to assist feature detection of aggregates. However, it is more difficult to detect aggregates than other particles because the aggregate image is very noisy, and the aggregates overlap or touch each other.

Multi-class segmentation is an important in image segmentation algorithms, which can simultaneously segment multiple different features of an aggregated image [3]. Common methods are: Thresholding, Region merging and split, Clustering, and Semantic segmentation. They employ distinct color blocks to differentiate locations based on image discontinuities, color or grayscale similarity, texture, and other characteristics [4]. The Region-growing [5] is typically effective at segmenting smooth areas of aggregate images, and yet the algorithm suffers from severe under-segmentation when aggregate particles are adhesion. The Watershed segmentation [6] can be applied for the images of densely packed aggregate, but there is over-segmentation at arris of polygonal aggregates. The Clustering algorithm [7] is good at segmenting the aggregate images with clear edges, but the aggregate overlapping problem cannot be resolved. The Semantic segmentation [8] might solve the aggregate touching problem; but, the aggregate surface texture will affect the segmentation results if the dataset cannot cover all the situations. However, creating a database of images with various aggregate rough texture features is challenging. The Thresholding is a computationally simple algorithm, and the features of the image are usually at the valleys or peaks of the histogram. This capability can be exploited to differentiate aggregate surface textures and edges [9]. Multi-thresholding (MT) easily separates contacting aggregates compared to Single-thresholding, while preserving details such as surface roughness, grain edges, etc. [10]. Since the MT is not affected by gray-scale similarity, it is more robust. Multiple Entropy Thresholding (MET) [11-12] is a popular method for automatic threshold determination, besides Otsu [13]. The MET is more efficient than Otsu, it determines the thresholds through entropy, and the entropies frequently employed for multi-class image segmentation are Kapur [14], Minimum-cross [15] and Renyi [16]. Therefore, the MET is utilized as one of the primary linkages in the suggested model in this paper. However, when applying the exhaustive method, the MET must test each threshold combination one by one in order to pick the optimal thresholds suitable for image segmentation. As a result, the more thresholds there are, the lower the operational efficiency.

The swarm intelligence optimization method learns the population's cooperative behavior in order to discover the target, and adopts a distributed iterative convergence strategy to achieve parameter optimization [17]. Compared with the exhaustive method, it can not only greatly reduce the time for MET to determine the threshold, but also does not degrade operating performance when the amount of thresholds grows [18-19]. Currently popular algorithms of this type are: Whale Optimization Algorithm (WOA) [20], Bacterial Foraging Algorithm (BFO), Gray Wolf Optimization (GWO) [21], Artificial Bee Colony Algorithm (ABCO), Particle Swarm Optimization (PSO) [22], Bat Algorithm (BAT), Mayfly Algorithm (MA) [23], Antlion Algorithm (ALO), Butterfly Optimization Algorithm (BOA) and Sparrow Search Algorithm (SSA) [24] etc. The precision, stability, convergence speed of algorithm optimization is affected by the population position, pathfinding and local optima. For example, the population of the GWO is distributed according to grade, resulting in good optimization precision. Whale spiral search in the WOA, which makes the WOA iterate faster. The SSA

stores the sparrow's position in the matrix to avoid repeated searches. And the population is divided into producers, scroungers, and vigilantes, each of which corresponds to two update methods, and the three kinds of sparrows are optimized at the same time, with high efficiency and robustness. But these algorithms have two disadvantages that lead to the performance degradation, that is, incomplete global search and falling into neighborhood optimum. For a more comprehensive search, chaotic map [25] is suggested, and Chen et al. [26] proposed reverse learning. For the local optimal solution, Levy flight [26] is suggested to jump out of the local area, and Liu et al. [25] made a Cauchy-Gauss mutation strategy. These evolutionary strategies are suitable for different optimization algorithms and objective functions; otherwise it is difficult to balance the optimization accuracy and convergence speed. Combining these performances, SSA [24] is currently a better optimization algorithm, and it has played a very good role in the parameter selection in the fields of path planning [27], production forecasting [28] and network selection [29]. Hence, this paper takes the SSA as one of the other main links of the proposed model, and optimizes the MET based on the improved SSA.

The following are the study's primary contributions:

1. An adaptive multi-class segmentation model for aggregate images, CSSA-MET, is suggested. CSSA can quickly and accurately help three METs to determine the thresholds and to improve the segmentation efficiency.

2. A Chaotic SSA is suggested, in which the chaotic map is combined with the sinusoidal dynamic weight and the elite mutation strategies, and it is firstly studied to promote the SSA's optimization accuracy and stability without reducing the SSA's speed. On the benchmark function tests, the CSSA outperforms the other seven similar algorithms.

3. Numerous aggregate image segmentation experiments demonstrate the feasibility and effectiveness of the CSSA-MET for segmenting aggregate images. To evaluate all methods comprehensively, a new parameter I based on segmentation accuracy and processing speed is constructed. According to the results, the CSSA optimized Renyi Entropy performs best for segmenting aggregated particles images.

The remainder of this work is presented: The Section 2 includes the MET and SSA. The CSSA-MET is explained in full in Section 3. Section 4 contains the CSSA and CSSA-MET tests. Finally, this investigation is summarized in Section 5.

2. Preliminaries

In this section, three METs are presented in Subsection 2.1, and SSA is introduced in Subsection 2.2.

2.1 Multiple Entropy Thresholding

The MET is a multi-class image segmentation algorithm. Its principle is to find a set of values to make the total information entropy of the image reach the extreme value. These values are the segmentation thresholds. Divide the histogram utilizing thresholds, then translate the result to each pixel in the image and assign closest gray value per pixel. The MET determines the thresholds through entropy, and the entropies frequently employed are Kapur [14], Minimum-cross [15] and Renyi [16], which calculate different amounts of information.

Assuming that the image size is $M \times N$, and the image is grayscaled into $0 \sim G$ levels, when the gray-scale value is i the number of pixels is n_i, and the probability i occurrence is $P_i = n_i/(M \times N)$. The gray-scale value range of the k-th area is $[g_{k-1}, g_k]$, $0 \leq g_{k-1} \leq g_k \leq L$. Then the average gray value of this area is u_k, and the probability sum of the gray-scale values

in this region is $\omega_k = \sum_{i=g_{k-1}}^{g_k} P_i$. The information of this areas is H_1, H_2, $\cdots$, and H_{K+1} respectively, then the information total is $E = H_1 + H_2 + \cdots + H_{K+1}$. Calculate the thresholds $g_{(1,2,\cdots,K)}$ that make the E reach the maximum or minimum value, as shown in **Fig. 1**. The mathematical expression of MET calculation thresholds is shown in **Table 1**.
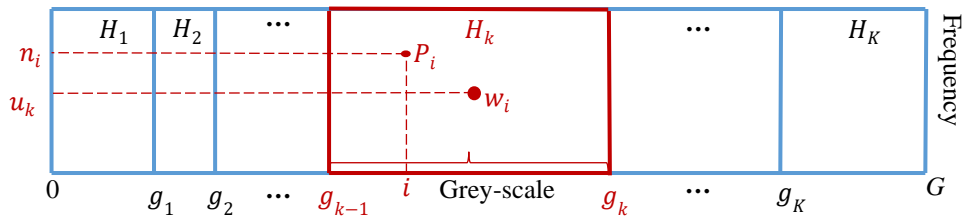

Fig. 1. Schematic diagram of MET determination thresholds.

Table 1. The thresholds determination methods of three METs

MET	Information value of the k-th region	Thresholds
Kapur	$H_k(g) = -\sum_{i=g_{k-1}}^{g_k} ln\left(\frac{P_i}{\omega_k}\right)\cdot\frac{P_i}{\omega_k}$	$g_{(1,2,\cdots,K)} = argmax\{E\}$
Minimum-cross	$H_k(g) = \sum_{i=g_{k-1}}^{g_k} i\cdot ln\left(\frac{i}{u_k}\right)\cdot n_i$	$g_{(1,2,\cdots,K)} = argmin\{E\}$
Renyi	$H_k(g) = \frac{1}{1-\alpha} ln\left(\sum_{i=g_{k-1}}^{g_k}\left(\frac{P_i}{\omega_k}\right)^\alpha\right), \alpha = 0.5$	$g_{(1,2,\cdots,K)} = argmax\{E\}$

Table 2 shows the differences in their segmented aggregate images when $K = 2$. It can be observed that the histogram fluctuates smoothly in some gray-scale intervals due to the aggregate's gray scale, but it is rich in extreme points, which are typical features of the aggregate image, such as edges and surface rough texture. When K is small, the accuracy is low, and as K increases, the MET detects more features.

Table 2. The results of the MET splitting two kinds of aggregate particles when $K = 2$

MET	**Kapur**		**Minimum-cross**		**Renyi**	
Image	Dark	Bright	Dark	Bright	Dark	Bright
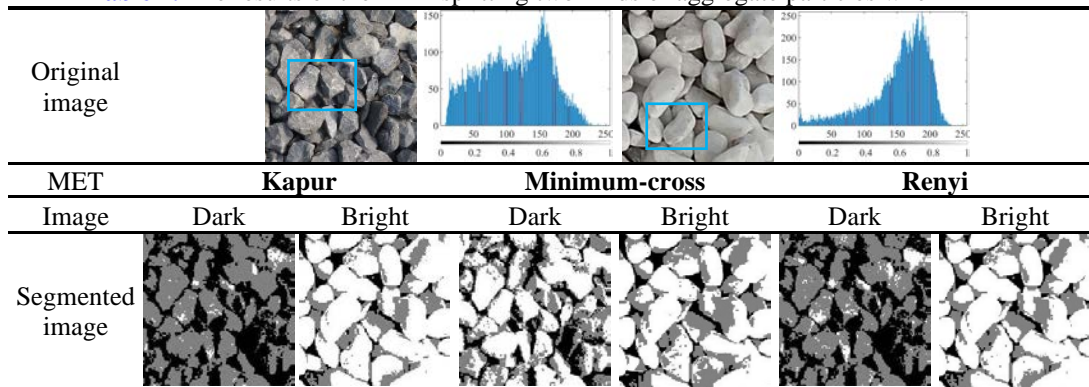
The dark aggregate image's brightness values are concentrated in dark area, and the histogram has only one clear valley. Kapur and Renyi Entropy detected the more brighter part details, while Minimum-cross Entropy identified the more darker part features. However, bright aggregate image's brightness values are concentrated in bright parts, and the histogram has no obvious valley. At this time, the focus of the three METs detection results is just the opposite. The major cause of this disparity is variance in the histogram. Since there are many extreme points in the histogram and their distance is close, even with only close thresholds,

there can be significant differences in results. As a result, the optimization techniques directly affect the quality of image segmentation.

2.2 Sparrow Search Algorithm

The SSA [24] is a recent optimization algorithm for mimicking sparrow behavior and has better convergence accuracy, speed and robustness. The SSA stores each sparrow's location $x_{i,j}$ in each dimension in a matrix, $i \in [1, n], j \in [1, d]$, n is the number of sparrows and d is the dimension.

Sparrows are divided into producers, scroungers and vigilantes. Producers are the core of the team, determine the direction of population movement, and are also the key to global search. The scroungers affect local convergence, and vigilante can react quickly when in danger. Each sparrow corresponds to two position update formulas, and these three kinds of sparrows update their positions respectively according to **Table 3**.

Table 3. Sparrow location update method

Sparrow	Update method	Parameter
Producers	$x_{i,j}^{t+1} = \begin{cases} x_{i,j}^{t} \cdot exp(-i/(\alpha \cdot T_{max})) & R_2 < ST \\ x_{i,j}^{t} + Q \cdot L & R_2 \geq ST \end{cases}$	t and T_{max}: the current and maximal iteration count R_2: warning value in $(0,1]$ ST: safety value in $[0.5, 1]$
Scroungers	$x_{i,j}^{t+1} = \begin{cases} x_{best}^{t+1} + \left\| x_{i,j}^{t} - x_{best}^{t+1} \right\| \cdot A^+ \cdot L & i \leq n/2 \\ Q \cdot exp\left((x_{worst}^{t} - x_{i,j}^{t})/i^2 \right) & i > n/2 \end{cases}$ $A^+ = A^T(AA^T)^{-1}$	α: constant in $(0,1)$ Q: random value L: the all-1 matrix of order $1 \times d$ φ_{best}: optimal φ φ_{worst}: worst φ
Vigilantes	$x_{i,j}^{t+1} = \begin{cases} x_{best}^{t} + \beta \cdot \left\| x_{i,j}^{t} - x_{best}^{t} \right\| & f_i > f_{best} \\ x_{i,j}^{t} + K \cdot \frac{\left\| x_{i,j}^{t} - x_{worst}^{t} \right\|}{(f_i - f_{\omega orst}) + \varepsilon} & f_i = f_{best} \end{cases}$	A: the matrix of order $1 \times d$, β: the step size control parameter $K \in [-1, 1]$: controls direction ε: a smallest constant

Fig. 2 left shows the optimization principle of the SSA. It is clear that the performance of the SSA is closely connected to sparrow's population dispersion, optimization pathway, and localized optimum.

To boost the SSA's effectiveness, Chen et al. [26] added Tent map, dynamic parameters, and Levy flight (CDLSSA) to the SSA, with increased accuracy but slower speed. Liu et al. [25] advocated a Cubic map and adaptive weight to optimize the SSA (CASSA). The speed of this algorithm was fast, but the accuracy was not greatly improved. At present, there is no single method that provides the optimal configuration of speed and precision.

3. Methods

This section the three evolution strategies of the CSSA are introduced in detail in Subsection 3.1, and the flow of the CSSA-MET is shown in Subsection 3.2.

3.1 CSSA

Chaotic Sparrow Search Algorithm (CSSA) makes targeted improvements to the three deficiencies of the SSA, corresponding to three evolutionary strategies. The optimization principle diagram of the CSSA is illustrated in **Fig. 2** right. The initial sparrow positions are

more evenly spread out, the optimization path is wider, and sparrows confined to a local area can successfully leap away from it.
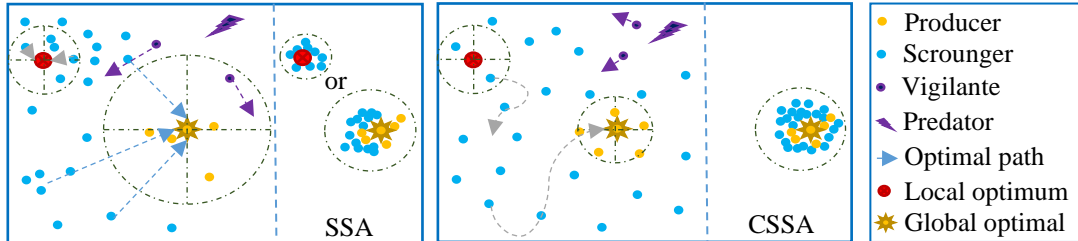

Fig. 2. SSA and CSSA optimization principle diagrams.

3.1.1 Chaotic map

Chaotic system is a definite nonlinear system, which has the characteristics of good uniformity, high randomness, fast speed and low cost. Therefore, chaos maps are often used to change the state of the system. The initial position of the sparrows in the SSA is stochastic, and if the sparrows gather, it hinders the worldwide search. As a result, we suggested to adopt a chaotic map at initialization. To scatter the sparrows so that they are evenly distributed globally. Piecewise map [30] is a chaotic map with high precision and good stability, which can be described as (1).

$$x' = \begin{cases} x(k)/P & P > x \geq 0 \\ 1 - (x(k) - 0.5)/(P - 0.5) & 0.5 > x \geq P \\ 1 + (x(k) - 0.5)/(P - 0.5) & 1 - P > x \geq 0.5 \\ (1 - x(k))/P & 1 > x \geq 1 - P \end{cases}, P \in (0,1) \neq 0.5 \qquad (1)$$

The chaotic sequences are shown in Fig. 3. The ordinate is the frequency of occurrence of x, which represents the uniformity of x, which is used in the SSA to represent the uniformity of the mapped sparrow position. Piecewise map has significant randomization, and this chaos sequence is most uniform when $P = 0.4$.
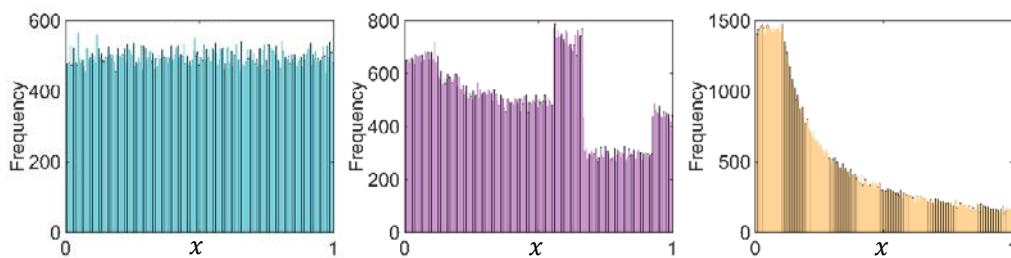

Fig. 3. Sequences of $P = 0.4, 0.6, 0.9$ after Piecewise chaotic map when $x(1) = 0.1$.

Since the range $[0, 1]$ of the chaotic map, it is required to translate into the target space's limits $[lb, ub]$ during the CSSA initialization phase.

3.1.2 Sinusoidal dynamic weight

Instance $y = e^{-x}$ has an impact on the producers. The traveling distance quickly shrunk as t rises. It lowers the capacity to do global searches, easier to enter the neighborhood optimum, which decreases the optimizing accuracy.

Therefore, this paper proposes a sinusoidal dynamic weight for adjusting the search range for the first time, which can be expressed as (2).

$$w = \begin{cases} \frac{1}{2}\left(w_{max} - sin\left(\frac{t\cdot\pi}{T_{max}} - \frac{T_{max}}{2}\right)\right) & t < \frac{T_{max}}{2} \\ w_{min} + sin(\frac{t\cdot\pi}{2\cdot T_{max}}) & t \geq \frac{T_{max}}{2} \end{cases} \tag{2}$$

Where, w_{max} and w_{min} are the initial and later weight respectively. After many experiments, when $w_{max} = 1$ and $w_{min} = -1$, the convergence effect is the best.

In the early iteration, w is large, population is scattered. In the later iteration, w is small, which helps the sparrow to converge. Introduce (2) into the position update of the producers, then becomes (3).

$$x_{i,j}^{t+1} = \begin{cases} x_{i,j}^t \cdot exp\left(-\frac{i}{\alpha\cdot T_{max}}\right) \cdot w & R_2 < ST \\ x_{i,j}^t + Q \cdot L & R_2 \geq ST \end{cases} \tag{3}$$

3.1.3 Elite mutation

The sparrows are trapped in a local optimum, and if it doesn't get out early, it will cause better solutions to be missed.

Therefore, an elite mutation that executes swiftly is put forward. Only at finish for every iteration, sort individual fitness values, select an elite sparrow with the best fitness value, and update its position according to (4).

$$x'_{best} = (ub - lb) \cdot randn + lb \tag{4}$$

Where, x'_{best} is the mutated position of the elite sparrow.

When the SSA becomes stalled inside the nearby region, it can easily leap out and continue to global search to increase the algorithm's performance. Even if this sparrow had converged to the global optimal solution, only changing the search path of one sparrow will not affect the final convergence result.

3.2 CSSA-MET

This paper proposes an adaptive multi-class segmentation model the CSSA-MET for aggregate images, which is composed of a swarm intelligence optimization algorithm CSSA and a multi-class segmentation algorithm MET. The flowchart of the CSSA-MET is shown in **Fig. 4**, and the purple font in the figure is the innovation point.
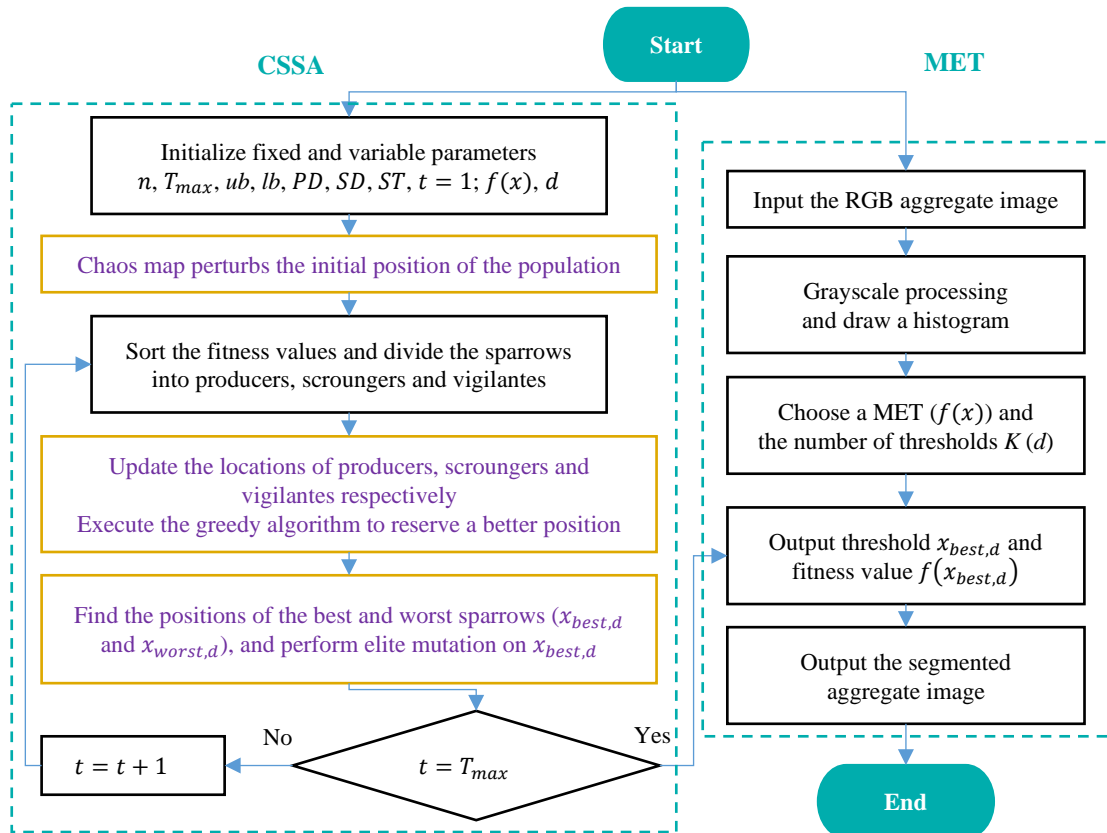
Fig. 4. Flowchart of adaptive multi-class segmentation model CSSA-MET.

4. Experiments

The benchmark function experiment for the optimization algorithm CSSA evaluation is in Subsection 4.1, and the evaluation experiment for the aggregate image adaptive multi-class segmentation model CSSA-MET is in Subsection 4.2.

Our studies are carried out with a computer outfitted with an Intel (R) Core (TM) i5-10400F @2.90 GHz CPU, 16 GB RAM and a 64-bit Win-10 operating system.

4.1 Performance of Optimization Algorithm CSSA

Benchmark functions are used to assess the performance of optimization algorithms. The capacity to locally converge is tested by the unimodal function, while the ability to globally explore is tested by the multimodal function.

The pertinent expressions are displayed in **Table 4**, and their versions are shown in **Fig. 5** at the dimension (D) is 2.

The CSSA is contrasted to the WOA [20], GWO [21], PSO [22], MA [23], SSA [24], CASSA [25], and CDLSSA [26]. The parameters are set in **Table 5**.

The accuracy, stability, and speed of the optimization method are taken into consideration while choosing the average value, standard deviation and time-consuming as assessment measures. Since the population's starting positions are stochastic, the average of 60 optimisation tests is utillized as the final evaluation result, these are provided in **Table 6**.

Table 4. Benchmark functions

Class	Function expression, argument range, optimal value
Uni-modal	$F_1(x) = \sum_{i=1}^{D} x_i^2$, $[-100,100]^D$, 0
	$F_2(x) = max\{|x_i|, 1 \le i \le D\}$, $[-100,100]^D$, 0
	$F_3(x) = \sum_{i=1}^{D}[(x_i - 1)^2 + 100(x_{i+1} - x_i^2)^2]$, $[-30,30]^D$, 0
Multi-modal	$F_4(x) = -\sum_{i=1}^{D} x_i \cdot sin(\sqrt{|x_i|})$, $[-500,500]^D$, $-418.9829D$
	$F_5(x) = -20\, exp\left(-0.2\sqrt{\frac{1}{D}\sum_{i=1}^{D} x_i^2}\right) - exp\left(\frac{1}{D}\sum_{i=1}^{D} cos(2\pi x_i)\right) + 20 + e$, $[-32,32]^D$, 0
	$F_6(x) = \frac{\pi}{D}\{10sin^2(y_1 \cdot \pi) + \sum_{i=1}^{D-1}(1 - y_i)^2 (10sin^2(y_{i+1} \cdot \pi) + 1) + \sum u(x_i, 10, 100, 4)\}$, $[-50,50]^D$, 0
	$y = (x + 5)/4$, $u(x, 10, 100, 4) = \begin{cases} 100 \cdot (\pm x - 10)^4 & |\pm x| > 10 \\ 0 & |x| \le 10 \end{cases}$
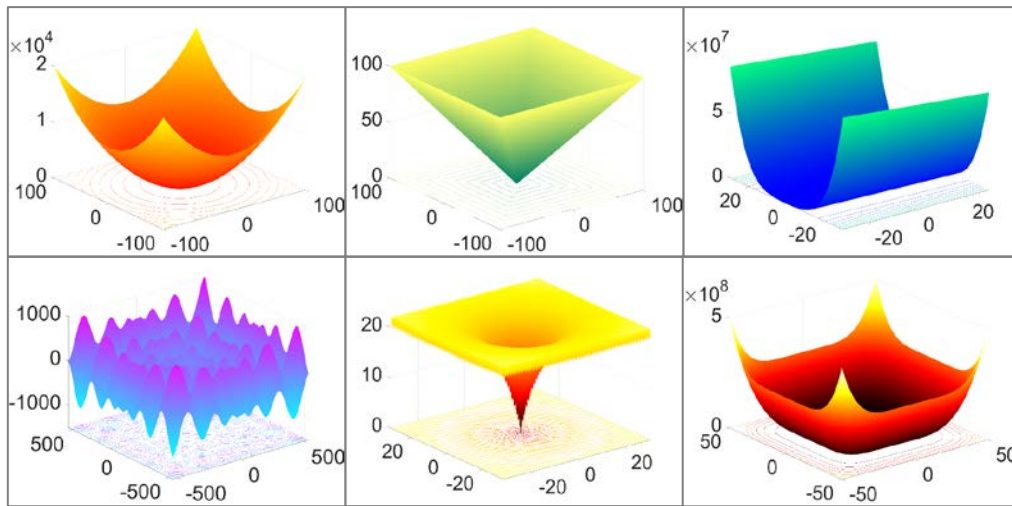
Fig. 5. 2-D representations of benchmark functions $F_1 \sim F_6$.

Table 5. Parameters of the optimization algorithms

Category	Algorithm	Parameter
Classic	WOA	$\alpha \in [0,2]$, $b = 1$, $l \in [-1,1]$
	GWO	α decreases linearly from 2 to 0, $r_1, r_2 \in [0,1]$
	PSO	$C_1 = C_2 = 1.5$, $\omega = 0.74$
	MA	$g = 1$, $gdamp = 1$, $\alpha_1 = 1$, $\alpha_2 = \alpha_3 = 1.5$
SSA series	SSA	$PD = 20\%$, $SD = 10\%$, $ST = 0.8$
	CDLSSA	$PD = 20\%$, $SD = 10\%$, $ST = 0.8$, $levy\ beat = 1.5$, $K = 2$
	CASSA	$PD = 20\%$, $SD = 10\%$, $ST = 0.8$, $S = 1$
	CSSA	$PD = 20\%$, $SD = 10\%$, $ST = 0.8$, $P = 0.4$, $w_{max} = 1$, $w_{min} = -1$
Uniform parameters		$n = 60$, $T_{max} = 600$, number of experiments is 60, $d = 30$

On the uni-modal and multi-modal functions in **Table 6**, the accuracy (*Avg*) and stability (*SD*) of the CSSA are always optimal. Although the speed (*T*/s) of the CSSA is not optimal, it is also close to the optimal value. The CASSA has weak stability, whereas the CDLSSA has

good accuracy and stability, but its speed is twice that of the CSSA, and only the CSSA achieves the optimal combination of speed and precision.

Table 6. Accuracy, stability and speed evaluation of eight optimization algorithms

| Function	WOA	GWO	PSO	MA	SSA	CDLSSA	CASSA	CSSA
				Average value (Avg)				
F_1	2.56×10^{-105}	3.14×10^{-43}	3.34×10^{-9}	3.23×10^{-8}	6.75×10^{-51}	$\mathbf{0}$	9.18×10^{-43}	$\mathbf{0}$
F_2	3.14×10^{1}	6.69×10^{-11}	1.62×10^{0}	4.79×10^{1}	7.95×10^{-15}	4.18×10^{-206}	5.70×10^{-10}	$\mathbf{0}$
F_3	2.71×10^{1}	2.67×10^{1}	2.53×10^{2}	6.53×10^{1}	1.32×10^{-3}	7.14×10^{-4}	1.09×10^{-3}	$\mathbf{4.59 \times 10^{-4}}$
F_4	-9.51×10^{3}	-6.04×10^{3}	-8.11×10^{3}	-1.05×10^{4}	-1.04×10^{3}	-1.86×10^{3}	-1.41×10^{3}	$\mathbf{-1.26 \times 10^{4}}$
F_5	4.09×10^{-15}	2.63×10^{-14}	6.56×10^{-1}	9.22×10^{-1}	9.47×10^{-16}	$\mathbf{8.88 \times 10^{-16}}$	1.01×10^{-15}	$\mathbf{8.88 \times 10^{-16}}$
F_6	1.53×10^{-2}	2.28×10^{-2}	9.34×10^{-2}	3.47×10^{-2}	6.63×10^{-7}	2.65×10^{-6}	4.74×10^{-7}	$\mathbf{2.06 \times 10^{-8}}$
				Standard deviation (SD)				
F_1	1.99×10^{-104}	4.35×10^{-43}	5.35×10^{-9}	1.49×10^{-7}	5.23×10^{-50}	$\mathbf{0}$	4.60×10^{-42}	$\mathbf{0}$
F_2	2.68×10^{1}	6.74×10^{-11}	7.40×10^{-1}	8.62×10^{0}	3.78×10^{-14}	$\mathbf{0}$	2.86×10^{-9}	$\mathbf{0}$
F_3	6.16×10^{-1}	6.32×10^{-1}	7.60×10^{2}	4.52×10^{1}	3.67×10^{-3}	1.87×10^{-3}	3.02×10^{-3}	$\mathbf{1.04 \times 10^{-3}}$
F_4	1.64×10^{3}	9.78×10^{2}	6.09×10^{2}	3.55×10^{2}	1.94×10^{3}	1.56×10^{2}	1.79×10^{3}	$\mathbf{5.67E\text{-}01}$
F_5	2.33×10^{-15}	3.53×10^{-15}	7.35×10^{-1}	6.03×10^{-1}	4.59×10^{-16}	$\mathbf{0}$	6.43×10^{-16}	$\mathbf{0}$
F_6	1.46×10^{-2}	1.06×10^{-2}	1.35×10^{-1}	7.04×10^{-2}	1.56×10^{-6}	5.68×10^{-6}	1.53×10^{-6}	$\mathbf{3.31 \times 10^{-7}}$
				Time-consuming (T)				
F_1	0.430	1.171	1.260	2.972	0.411	0.759	$\mathbf{0.399}$	0.407
F_2	0.425	1.174	1.202	2.970	0.414	0.743	$\mathbf{0.401}$	0.405
F_3	0.460	1.213	1.261	3.112	$\mathbf{0.432}$	0.812	0.465	0.444
F_4	0.471	1.215	1.295	3.125	$\mathbf{0.426}$	0.773	0.468	0.454
F_5	0.442	1.201	1.250	3.098	$\mathbf{0.412}$	0.735	0.416	0.446
F_6	0.924	1.661	1.763	4.384	0.902	1.556	0.900	$\mathbf{0.874}$
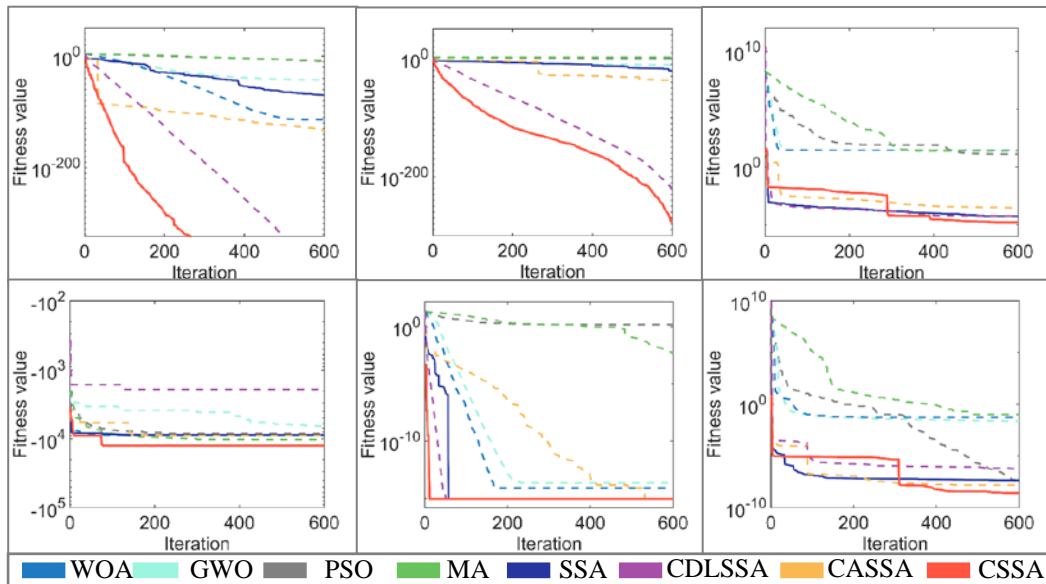
Fig. 6. Convergence curves of eight optimization algorithms on $F_1{\sim}F_6$.

The iteration curves of the eight optimization methods are displayed in **Fig. 6** for evaluation of the beneficial effects of these three evolutionary strategies on the CSSA. The first is chaotic mapping, which is reflected in the iteration curves of $F_3{\sim}F_6$. The population's starting position

is more uniform, which makes the initial value of the CSSA better. The second is the dynamic weight, it is reflected at $F_1 \sim F_2, F_6$, and search range is wider, so that the optimal solution of the CSSA is continuously updated, and it converges to the global optimum in later iterations. Finally, the elite mutation is reflected in some broken lines on F_1, F_3, F_4 and F_6. When they fall into a local optimum, they can effectively escape and improve the solution's accuracy.

Wilcoxon rank-sum test [31] is utilized to compare the significant distinction between two samples. This sample size in **Table 6** is small. In order to avoid unreliable results, samples with $D = 2,60$ were added to the test. **Table 7** displays the results. Bold words in the table indicate significant differences ($P - value \leq 0.05$).

Table 7. Wilcoxon test of CSSA vs. other optimization algorithms

Evaluation	Avg	SD	T
WOA	$\mathbf{2.30 \times 10^{-3}}$	$\mathbf{5.30 \times 10^{-4}}$	6.89×10^{-1}
GWO	$\mathbf{3.72 \times 10^{-3}}$	$\mathbf{2.45 \times 10^{-3}}$	$\mathbf{1.25 \times 10^{-3}}$
PSO	$\mathbf{8.47 \times 10^{-4}}$	$\mathbf{2.38 \times 10^{-5}}$	$\mathbf{4.30 \times 10^{-4}}$
MA	$\mathbf{5.49 \times 10^{-3}}$	$\mathbf{3.62 \times 10^{-4}}$	$\mathbf{1.74 \times 10^{-5}}$
SSA	3.26×10^{-1}	$\mathbf{3.59 \times 10^{-2}}$	7.93×10^{-1}
CDLSSA	6.87×10^{-1}	8.97×10^{-1}	$\mathbf{2.21 \times 10^{-2}}$
CASSA	3.57×10^{-1}	$\mathbf{3.96 \times 10^{-2}}$	8.76×10^{-1}

It can be seen that there are significant differences between the CSSA and WOA, GWO, PSO, and MA, except for *T* of the WOA. This shows that the CSSA is far superior to these four algorithms in accuracy (*Avg*) and stability (*SD*), and the CSSA is similar to the WOA in speed (*T*). Similarly, CSSA is much better than SSA and CASSA in stability (*SD*), and much better than CDLSSA in speed (*T*).

In addition, it can also be seen that the SSA, CDLSSA, CASSA and CSSA are similar (no bold). In terms of accuracy and stability, the CDLSSA is the best, followed by the CASSA, and finally the SSA. In terms of speed, the CASSA is the best, followed by the SSA, and the CDLSSA is the worst. Combining these conclusions **Table 6** shows that the CSSA has maximum accuracy, stability and also has a faster convergence speed.

4.2 Evaluation of Segmentation Model CSSA-MET

The MET is utilized as the optimization algorithm's objective function, and they are merged with the CSSA and SSA one by one to form six techniques, including three CSSA-METs and three SSA-METs. Simultaneously, Fuzzy C-means (FCM) is compared.

The 100+ aggregate image tests are obtained in the Key Laboratory of Road Construction Technology and Equipment, and **Fig. 7** displays five of them.

From the point of view of the histogram, they contain abundant glitch-like extreme points, and these extreme points are close in distance, which are the characteristics of aggregates. When the surface texture is rougher, although the threshold is similar, it might lead to a decrease in roughness, so the optimization algorithm's effectiveness will affect the segmentation precision.

From the perspective of aggregate characteristics, these particles have different characteristics such as shape, color, size, edge and surface rough texture. The features are used to evaluate gravel and pebbles, size aggregates, calculate sanding time, and detect parent rock type. During image processing, the quantity K of thresholds is decided upon in accordance with needs. $K = 2 \sim 6$ in relevant literatures, **Table 7** displays partial results of the CSSA-MET segmented aggregate images when $K = \{2,4,6\}$.
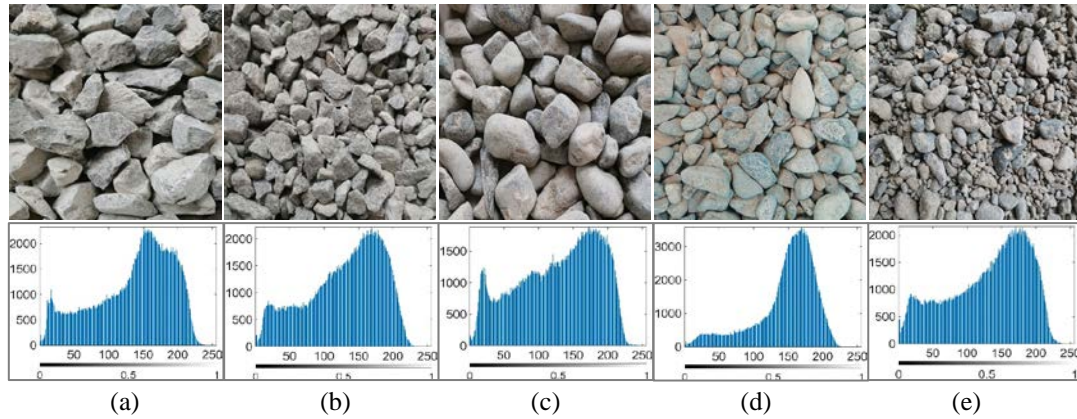
Fig. 7. Five aggregate images and their histograms.

Because in Subsection 4.1, the CSSA only iterates 200 times on the 30-dimensional function to complete the convergence. After many experiments, only 100 iterations of the CSSA-MET efficiently segment images. The remaining parameters are identical to those used in the prior section, and just 100 repetitions are required to reduce segmentation time while maintaining accuracy.

From a subjective point of view, when $K = 2$, the FCM segmentation effect is the best, second the Renyi. The MET's precision continues to improve at $K = 4$, while the FCM becomes increasingly unstable. When $K = 6$, Renyi segmented contact or overlapping aggregate particles performed well, second the Kapur, while the Minimum-cross brightness is higher. The grey- scale value divergences are severe even though the FCM's edges are visible.

Table 8. Partial results of CSSA-MET segmentation of aggregate images

Overall, the CSSA-MET outperforms the SSA-MET on the segmentation of aggregate images because the CSSA can obtain more accurate thresholds. The criterion for measuring optimization method's accuracy is whether optimized objective function can obtain a better fitness value. **Table 9** displays the fitness values and corresponding thresholds obtained by the

CSSA and SSA at $K = 6$, the bolder of the two is superior. The higher the fitness value of Kapur and Renyi in **Table 1**, the better, while Minimum-cross is the opposite. The CSSA:SSA ratio for obtaining optimal values is 9:0 (**Table 9**), demonstrating that the CSSA must have superior capabilities. Compared with the SSA-MET, the CSSA-MET has a more accurate threshold for segmenting images.

Table 9. Thresholds determined by CSSA-MET and their corresponding fitness values

Image	Parameter	Kapur		Minimum-cross		Renyi	
		SSA	CSSA	SSA	CSSA	SSA	CSSA
(a)	Thresholds	83 156 43 191 103 131	**69 168 110 199 137 36**	33 123 148 180 89 46	**123 96 185 153 32 66**	41 200 136 93 73 169	**148 185 78 225 41 114**
	Fitness	24.1227	**24.2284**	133205.7494	**121076.1347**	24.3861	**24.5142**
(c)	Thresholds	39 192 131 89 69 161	**74 231 119 190 153 46**	160 32 183 132 61 97	**88 151 57 30 181 119**	164 229 145 188 37 97	**94 227 55 130 192 161**
	Fitness	24.1205	**24.4108**	127944.5518	**123043.8349**	24.3552	**24.6649**
(e)	Thresholds	36 193 127 85 64 163	**33 64 124 157 193 93**	177 138 112 87 57 29	**122 88 26 56 184 154**	127 217 102 189 58 157	**76 188 157 221 42 117**
	Fitness	24.1677	**24.2632**	139618.2252	**133274.0496**	24.3328	**24.5365**

As the image size in **Table 8** is too small to see the difference between the CSSA-MET and SSA-MET segmentation results, the local regions of (c) are intercepted when $K = 6$. They are aggregate surface roughness, texture and edge, respectively, and each local image contains at least two main features. **Table 10** shows their segmentation results. It can be seen that the segmented images of the CSSA-MET contain more detailed features, while the results of the SSA-MET lose a lot of specifics, particularly roughness.

Table 10. Partial local results for CSSA-MET segmentation of aggregate images

Combining **Table 10** with the data of (c) in **Table 9**, it can be seen that even if the thresholds are not significantly different, it can cause a large difference in results. This demonstrates that the CSSA's effectiveness is critical for segmentation models.

The above is a subjective evaluation, and the image segmentation algorithm also needs a comprehensive objective evaluation. The similarity between the segmentation result and the ground-truth must be compared in order to assess the segmented image's reliability. Since the eye couldn't mark the true under each K, the segmentation results are contrasted to the original images.

The segmentation results are contrasted with the original image since the eye was unable to distinguish the real under each K.

The Peak Signal to Noise Ratio (*PSNR*), Structure Similarity (*SSIM*), Feature Similarity (*FSIM*) and the average time (*T*) to segment an image are made as assessment criteria. Relevant expressions are shown in **Table 11**.

Table 11. Image quality evaluation index

Index	Expression	Parameter
PSNR	$PSNR = 20\,log_{10}(255 \cdot \sqrt{\frac{M \times N}{\sum\sum(f-\hat{f})^2}})$	$M \times N$: image size f: original image $\hat{f}$: segmented image
SSIM	$SSIM(I,\hat{I}) = \frac{(2\mu_f\mu_{\hat{f}}+C_1) \times (2\sigma_{f,\hat{f}}+C_2)}{(\mu_f{}^2+\mu_{\hat{f}}{}^2+C_1) \times (\sigma_f{}^2+\sigma_{\hat{f}}{}^2+C_2)}$	μ: gray average σ: gray standard deviation C: constant, take $C_1 = C_2 = 6.45$
FSIM	$FSIM = \frac{\sum S_L \times PC_m}{\sum PC_m}, \quad S_L(w) = S_{PC}S_G,$ $S_{PC} = \frac{2PC_1PC_2+T_1}{PC_1^2+PC_2^2+T_1}, \quad S_G = \frac{2G_1G_2+T_2}{G_1^2+G_2^2+T_2}$ $PC_m = max(PC_1, PC_1)$	S_L: similarity score PC: phase consistency G: image gradient T: constant, take $T_1 = 0.85$, $T_2 = 160$

Greater information and smaller noise levels are indicated by a higher *PSNR* score; $SSIM \in [0, 1]$, the more similar the segmented picture is to the original image, the higher the *SSIM* value; $FSIM \in [0, 1]$, the tinier the feature difference between the image before and after segmentation, the larger the *FSIM* value. Therefore, the higher the values of these three parameters, the better the segmentation results. The average values of sixty tests are utilized as the ultimate results because of the unpredictability of the optimization algorithm population's beginning position. The statistical data of the *PSNR*, *SSIM* and *FSIM* are shown in **Tables 12-14**. The bold font in these tables is the value of the superior assessment criterion between the CSSA and SSA

From an optimization perspective, when the CSSA is compared to the SSA, the better *PSNR* values ratio is 30:0 (**Table 12**), the better *SSIM* values ratio is 25:7 (**Table 13**), and the better *FSIM* values ratio is 27:4 (**Table 14**). This means the capabilities of the CSSA to optimize the MET has an advantage in aggregate image segmentation. And as the number of thresholds increases, these benefits are grown. Especially in terms of the *PSNR* values, the CSSA-MET is better than the SSA-MET, which shows that the CSSA-MET can segment more details, and is suitable for all kinds of aggregate images, with high robustness.

From the threshold perspective, when $K = 2$, the *PSNR* values of the FCM are the maximum, but under the influence of the gray-scale values of the clustering centers and neighborhood pixels, the FCM performs worse and worse when $K = 4, 6$. On the contrary, the

performance of the CSSA-Renyi Entropy has been outstanding, achieving the best *PSNR* values at $K = 4, 6$, following Kapur, although Minimum-cross's results are slightly worse, but also better than the FCM. Similarly, on the *SSIM* and *FSIM* values, the CSSA-MET has achieved better results, and the FCM is similar to the above conclusion. These are the difference between the three METs in aggregate image segmentation.

Table 12. *PSNR* values

Image	K	Kapur		Minimum-cross		Renyi		FCM
		SSA	CSSA	SSA	CSSA	SSA	CSSA	
(a)	2	12.2	12.2	11.7	11.7	12.9	12.9	14.1
	4	16.5	**16.6**	15.1	**15.3**	17.2	**17.4**	11.5
	6	18.4	**20.2**	15.5	**18.1**	21.4	**22.3**	10.1
(b)	2	13.0	13.0	12.2	12.2	13.3	13.3	13.3
	4	16.8	**17.0**	14.5	**14.6**	17.8	**18.1**	12.5
	6	18.8	**20.1**	15.2	**16.6**	20.5	**21.8**	8.55
(c)	2	13.2	13.2	12.1	12.1	13.5	13.5	13.4
	4	16.9	**17.2**	14.8	**15.1**	17.7	**18.7**	12.1
	6	20.8	**21.7**	15.9	**16.4**	21.0	**22.1**	10.4
(d)	2	10.6	10.6	11.9	11.9	10.9	10.9	13.3
	4	16.2	**16.7**	14.7	**14.8**	17.5	**17.7**	11.2
	6	18.6	**20.2**	16.2	**17.5**	20.4	**21.6**	10.5
(e)	2	12.7	12.7	11.9	11.9	13.1	13.1	13.4
	4	16.5	**16.6**	14.4	**14.6**	17.6	**17.7**	10.2
	6	17.6	**19.8**	15.0	**17.0**	21.2	**22.8**	9.93

Table 13. *SSIM* values

Image	K	Kapur		Minimum-cross		Renyi		FCM
		SSA	CSSA	SSA	CSSA	SSA	CSSA	
(a)	2	0.308	**0.309**	**0.307**	0.306	0.321	0.321	0.330
	4	0.500	**0.502**	0.505	**0.508**	**0.511**	0.510	0.190
	6	**0.609**	0.606	0.601	**0.617**	0.614	**0.616**	0.041
(b)	2	0.350	0.350	0.344	0.344	0.358	0.358	0.358
	4	0.551	**0.552**	0.550	**0.552**	0.559	**0.562**	0.068
	6	0.657	**0.659**	0.650	**0.664**	0.657	**0.663**	0.032
(c)	2	0.312	0.312	0.307	0.307	0.318	0.318	0.317
	4	**0.490**	0.488	0.488	**0.491**	**0.500**	0.486	0.217
	6	0.577	**0.579**	0.596	**0.603**	0.582	**0.592**	0.144
(d)	2	0.317	0.317	0.340	0.340	0.329	0.329	0.341
	4	**0.499**	0.497	**0.511**	0.509	0.500	**0.502**	0.098
	6	0.594	**0.597**	0.608	**0.610**	0.596	**0.601**	0.078
(e)	2	0.442	0.442	0.439	0.439	0.454	0.454	0.454
	4	0.634	**0.635**	0.631	**0.636**	0.646	**0.647**	0.113
	6	0.715	**0.726**	0.712	**0.733**	0.734	**0.738**	0.075

Table 15 shows the standard deviation (*SD*) of the CSSA-MET and SSA-MET in 60 experiments, which can measure the stability of the algorithm, and the *SD* value is inversely proportional to the stability. Generally, the stability is the highest when $K = 2$. As the K value increases, the *SD* value increases and the stability decreases. The figure of merit ratio of the

CSSA-MET and SSA-MET is 19:8, indicating that the CSSA-MET has better stability.

Table 14. *FSIM* values

Image	K	Kapur		Minimum-cross		Renyi		FCM
		SSA	CSSA	SSA	CSSA	SSA	CSSA	
(a)	2	0.722	0.722	**0.719**	0.718	0.734	0.734	0.742
	4	0.868	**0.870**	0.870	**0.872**	0.872	**0.874**	0.741
	6	0.916	**0.919**	0.905	**0.917**	0.919	**0.924**	0.632
(b)	2	0.756	0.756	0.745	0.745	0.761	0.761	0.772
	4	0.892	**0.893**	0.878	**0.880**	0.896	**0.897**	0.758
	6	0.928	**0.935**	0.913	**0.924**	0.930	**0.939**	0.666
(c)	2	0.723	0.723	0.716	0.716	0.724	0.724	0.723
	4	**0.862**	0.861	0.856	0.859	**0.866**	0.860	0.721
	6	0.903	**0.907**	0.899	**0.907**	0.901	**0.913**	0.628
(d)	2	0.728	0.728	**0.751**	0.750	0.737	0.737	0.744
	4	0.872	**0.874**	0.865	0.865	0.873	**0.875**	0.690
	6	0.920	**0.925**	0.905	**0.907**	0.916	**0.926**	0.608
(e)	2	0.801	0.801	0.794	0.794	0.808	0.808	0.806
	4	0.908	**0.909**	0.898	**0.902**	0.915	**0.916**	0.704
	6	0.936	**0.947**	0.925	**0.940**	0.948	**0.956**	0.654

Table 15. *SD* values

Para-meter	K	Kapur		Minimum-cross		Renyi		FCM
		SSA	CSSA	SSA	CSSA	SSA	CSSA	
PSNR	2	4.61×10^{-2}	$\mathbf{4.48 \times 10^{-2}}$	$\mathbf{5.69 \times 10^{-2}}$	5.83×10^{-2}	4.83×10^{-2}	$\mathbf{4.79 \times 10^{-2}}$	2.28×10^{-3}
	4	0.36	**0.34**	0.31	**0.26**	**0.51**	0.54	4.28
	6	**1.31**	1.35	**0.800**	1.66	2.14	**1.76**	35.51
SSIM	2	6.29×10^{-4}	$\mathbf{5.92E-04}$	9.03×10^{-4}	$\mathbf{8.85 \times 10^{-4}}$	$\mathbf{5.63 \times 10^{-4}}$	5.70×10^{-4}	2.65×10^{-4}
	4	$\mathbf{2.97 \times 10^{-3}}$	3.01×10^{-3}	5.25×10^{-3}	$\mathbf{3.06 \times 10^{-3}}$	5.01×10^{-3}	$\mathbf{4.88 \times 10^{-3}}$	0.65
	6	1.27×10^{-2}	$\mathbf{1.12 \times 10^{-2}}$	$\mathbf{1.18 \times 10^{-2}}$	1.23×10^{-2}	2.05×10^{-2}	$\mathbf{1.28 \times 10^{-2}}$	3.12
FSIM	2	1.18×10^{-3}	$\mathbf{1.09 \times 10^{-3}}$	1.17×10^{-3}	$\mathbf{1.15 \times 10^{-3}}$	8.80×10^{-4}	$\mathbf{8.66 \times 10^{-4}}$	5.21×10^{-4}
	4	3.50×10^{-3}	$\mathbf{3.11 \times 10^{-3}}$	5.12×10^{-3}	$\mathbf{2.77 \times 10^{-3}}$	$\mathbf{2.70 \times 10^{-3}}$	3.26×10^{-3}	0.61
	6	1.02×10^{-2}	$\mathbf{8.89 \times 10^{-3}}$	1.02×10^{-2}	$\mathbf{7.70 \times 10^{-3}}$	1.40×10^{-2}	$\mathbf{8.86 \times 10^{-3}}$	3.69

The average time-consuming of image segmentation of each algorithm is statistically calculated in **Table 16**. The ratio of the better *T* values of the CSSA-MET to the SSA-MET is 5:4. the CSSA's three techniques did not affect the SSA's efficiency, and the CSSA was occasionally faster than the SSA. The key cause is the aggregate histogram's particularity, it has a lot of extreme points, resulting in a lot of local optimum in the optimization process. Elite mutation allows the SSA to easily slip into these locals, but the CSSA can jump out of them in time. As a result, the CSSA-MET is better suited for segmenting aggregate images.

Table 16. *T* values

K	Kapur		Minimum-cross		Renyi		FCM
	SSA	CSSA	SSA	CSSA	SSA	CSSA	
2	2.024 s	**1.789 s**	**1.762 s**	1.798 s	1.775 s	**1.745 s**	1.752 s
4	**1.806 s**	1.816 s	1.842 s	**1.837 s**	**1.789 s**	1.823 s	5.168 s
6	1.873 s	**1.862 s**	1.953 s	**1.929 s**	**1.836 s**	1.854 s	8.589 s

For the same segmentation method, it is not always optimal in the four parameters, which brings trouble to the practical evaluation of the algorithms.

The segmentation models' line graphs for the four evaluation parameters are displayed in **Fig. 8**. A method cannot achieve the optimal values on all parameters at the same time, therefore, these four indicators are normalized and fused into a new weight parameter I, $I \in [0, 1]$. The algorithm's advantage increases with increasing I value. The I value can be calculated by (5), and the I value statistics of all algorithms are summarized in **Table 17**.

$$I = \sum \sum \frac{|\overline{I_{K,P}} - worst_{K,P}|}{N_{K,P} \cdot \Delta I_{K,P}} \tag{5}$$

Where, $P = PSNR, SSIM, FSIM, T$ are the evaluation parameters, $K = 2, 4, 6$, $\Delta I_{K,P} = |best_{K,P} - worst_{K,P}|$, $worst$ is the worst value, $best$ is the optimal value, and $N_{K,P}$ is the number of (K, P). In this study, $N_{K,P} = 3 \times 4 = 12$.
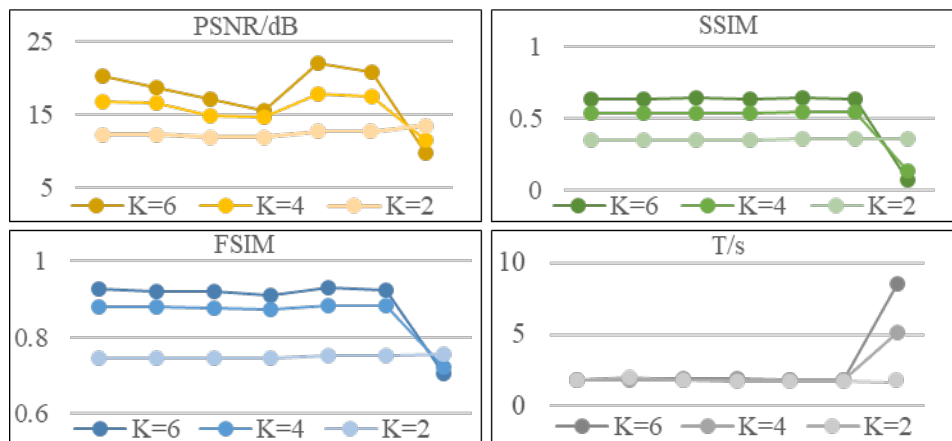
Fig. 8. The segment methods' line graph for the four assessment criteria. The abscissa corresponds to the CSSA-Kapur, SSA-Kapur, CSSA-Minimum-cross, SSA-Minimum-cross, CSSA-Renyi, SSA-Renyi, and FCM from left to right.

In Subsection 4.1, the Wilcoxon rank sum test showed that the SSA, CASSA, CDLSSA and CSSA were similar. Therefore, the comprehensive evaluation results of the CASS-MET and CDLSSA-MET are added in **Table 17**.

Table 17. I values

Algorithm	SSA	CDLSSA	CASSA	CSSA
Kapur	0.662422	0.706977	0.710967	0.746250
Minimum-cross	0.637545	0.657510	0.665500	0.692467
Renyi	0.784693	0.796192	0.800182	**0.825743**
FCM		0.272944		

In **Table 17**, from a horizontal perspective, the I value of the CSSA-MET is always higher. Followed by the CASSA-MET, the CDLSSA-MET is affected by the T value, the comprehensive evaluation parameters are low, and the result of the SSA-MET is not very ideal. Vertically, the I value of Renyi Entropy is always higher. This is followed by Kapur Entropy and finally by Minimum-cross Entropy.

On the whole, the CSSA-Renyi Entropy has the strongest realizability for segmenting aggregate images. The result of the CSSA-Renyi Entropy segmenting aggregate image (e) when $K = 6$ and the segmentation histogram are shown in **Fig. 10**. It can be seen that the threshold selection is reasonable, and the surface texture and edge of the aggregate are well preserved.
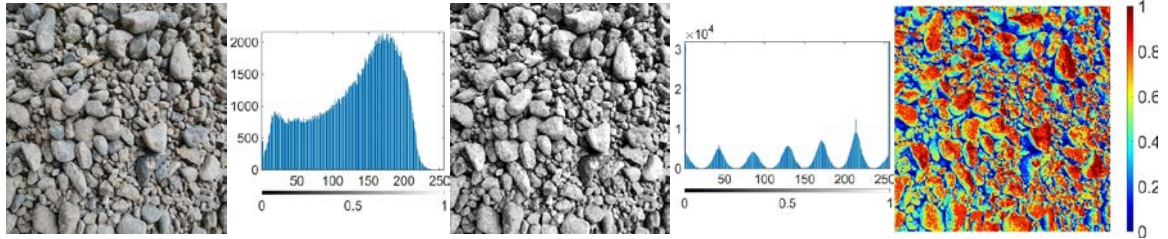

Fig. 9. CSSA-Renyi Entropy segmentation result and segmentation histogram of aggregate image (e) when $K = 6$.

5. Conclusion

This paper proposes an adaptive multi-class image segmentation model for multi-aggregate images based on the Chaotic SSA, named CSSA-MET, it aims to overcome the shortcoming of MET's unbalanced running time and accuracy in multi-class segmentation of aggregate images. Firstly, the CSSA combines Chaotic map, sinusoidal dynamic weights and elite mutation to improve the performance of the SSA. Benchmark function experiment and Wilcoxon rank-sum test verify better optimization ability of the CSSA. Then, the CSSA is utilized to quickly determine the correct MET thresholds. In the various segmentation experiments, the CSSA-MET is proved that can segment aggregate images in more aggregate details. And finally, a normalized weight parameter I is proposed to evaluate the performance of segmented images, which integrates *PSNR*, *SSIM*, *FSIM* and *T*, and all five indicators show that the CSSA-MET is more effective than the SSA-MET and FCM, and among the three METs, the CSSA optimized Renyi Entropy performs is the best, achieving the best balance between speed and accuracy, and effectively retaining rough surface texture and edge features.

In future work, we will explore the image segmentation focus of each method and try to fuse them to achieve parallel classification of multiple aggregate features. In addition, the three evolutionary strategies, the CASSA and CASSA-MET models in this paper can be used in similar fields and have broad application prospects.

References

[1] Y. Zhou, H. Jin, Wang B, "Modeling and mechanical influence of meso-scale concrete considering actual aggregate shapes," *Construction and Building Materials*, vol. 228, pp. 116785, Dec. 2019. Article (CrossRef Link)

[2] K. Ma, X. Huang, "The morphological characteristics of brick-concrete recycled coarse aggregate based on the digital image processing technique," *Journal of Building Engineering*, vol. 44, pp.1032192, Dec. 2021. Article (CrossRef Link)

[3] Y. Wang, M. Shabaninejad, R. Armstrong, et al., "Deep neural networks for improving physical accuracy of 2D and 3D multi-mineral segmentation of rock micro-CT images," *Applied Soft Computing*, vol. 104, pp. 107185, Jun. 2021. Article (CrossRef Link)

[4] R. Grewal, S. Kasana, "Hyperspectral image segmentation: a comprehensive survey," *Multimed Tools Appl.*, vol. 2022, pp.1-54, Oct. 2022. Article (CrossRef Link)

[5]   Z. Cheng and J. Wang, "Improved region growing method for image segmentation of three-phase materials," *Powder Technol.*, vol. 368, pp. 80-89, May, 2020. Article (CrossRef Link)

[6]   Q. Guo, Y. Wang, and S. Yang, et al., "A method of blasted rock image segmentation based on improved watershed algorithm," *Sci. Rep.*, vol. 12, Article no.7143, May, 2022.
Article (CrossRef Link)

[7]   Y. Wang, W. Tu, and H. Li, "Fragmentation calculation method for blast muck piles in open-pit copper mines based on three-dimensional laser point cloud data," *Int. J. Appl. Earth Obs.*, vol. 100, pp. 102338, Aug. 2021. Article (CrossRef Link)

[8]   Y. Liu, Z. Zhang, X. Liu, et al, "Efficient image segmentation based on deep learning for mineral image classification," *Advanced Powder Technology*, vol. 32, no. 10, pp. 3885-3903, Oct. 2021.
Article (CrossRef Link)

[9]   Y. Ju, H. F. Sun, and M. X. Xing, et al., "Numerical analysis of the failure process of soil-rock mixtures through computed tomography and PFC3D models," *Int. J. Coal Sci. Technol.*, vol. 5, no. 2, pp. 126-141, Jan. 2018. Article (CrossRef Link)

[10] X. Liu, J. Yan, and X. Zhang, et al., "Numerical upscaling of multi-mineral digital rocks: Electrical conductivities of tight sandstones," *J. Petrol. Sci. Eng.*, vol. 201, pp. 108530, Jun. 2021.
Article (CrossRef Link)

[11] D. Zhao, L. Liu, F. Yu, et al., "Chaotic random spare ant colony optimization for multi-threshold image segmentation of 2D Kapur entropy," *Knowledge-Based Systems*, vol. 216, pp. 106510, Mar. 2021. Article (CrossRef Link)

[12] H. Gill, B. Khehra, A. Singh, et al., "Teaching-learning-based optimization algorithm to minimize cross entropy for Selecting multilevel threshold values," *Egyptian Informatics Journal*, vol. 20, no. 1, pp. 11-25. Mar. 2019. Article (CrossRef Link)

[13] C. Huang, X. Li, Y. Wen, "An OTSU image segmentation based on fruitfly optimization algorithm," *Alexandria Engineering Journal*, vol. 60, no. 1, pp. 183-188, Feb. 2021.
Article (CrossRef Link)

[14] P. Upadhyay, J. Chhabra, "Kapur's entropy based optimal multilevel image segmentation using crow search algorithm," *Applied soft computing*, vol. 97, pp. 105522, Dec. 2020.
Article (CrossRef Link)

[15] R. Chakraborty, R. Sushil, M. Garg, "An Improved PSO-Based Multilevel Image Segmentation Technique Using Minimum Cross-Entropy Thresholding," *Arab J Sci Eng.*, vol. 44, pp. 3005–3020, Jun. 2019. Article (CrossRef Link)

[16] L. Peng, D. Zhang, "An adaptive Lévy flight firefly algorithm for multilevel image thresholding based on Rényi entropy," *The Journal of Supercomputing*, vol. 78, no. 5, pp. 6875-6896, Oct. 2022.
Article (CrossRef Link)

[17] J. Tang, G. Liu and Q. Pan, "A Review on Representative Swarm Intelligence Algorithms for Solving Optimization Problems: Applications and Trends," *IEEE/CAA Journal of Automatica Sinica*, vol. 8, no. 10, pp. 1627-1643, Oct. 2021. Article (CrossRef Link)

[18] E. Houssein, E. Helmy, D. Oliva, et al., "Multi-level thresholding image segmentation based on nature-inspired optimization algorithms: a comprehensive review," *Metaheuristics in Machine Learning: Theory and Applications*, vol. 2021, pp. 239-265, Jul. 2021. Article (CrossRef Link)

[19] L. Ren, A. Heidari, Z. Cai, et al., "Gaussian kernel probability-driven slime mould algorithm with new movement mechanism for multi-level image segmentation," *Measurement*, vol. 192, pp. 110884, Mar. 2022. Article (CrossRef Link)

[20] S. Mirjalili and A. Lewis, "The whale optimization algorithm," *Adv. Eng. Softw.*, vol. 95, pp. 51-67, May, 2016. Article (CrossRef Link)

[21] S. Mirjalili, S. M. Mirjalili, and A. Lewis, "Grey wolf optimizer," *Adv. Eng. Softw.*, vol. 69, pp. 46-61, Mar. 2014. Article (CrossRef Link)

[22] J. Kennedy and R. Eberhart, "Particle swarm optimization," in *Proc. of ICNN'95-International Conference on Neural Networks*, Perth, WA, Australia, pp. 1942-1948, 1995.
Article (CrossRef Link)

[23] K. Zervoudakis and S. Tsafarakis, "A mayfly optimization algorithm," *Comput. Ind. Eng.*, vol. 145, pp. 106559, Jul. 2020. Article (CrossRef Link)

[24] J. K. Xue and B. Shen, "A novel swarm intelligence optimization approach: sparrow search algorithm," *Syst. Sci. Control Eng.*, vol. 8, no. 1, pp. 22-34, Dec. 2020. Article (CrossRef Link)

[25] G. Liu, C. Shu, and Z. Liang, et al., "A modified sparrow search algorithm with application in 3d route planning for UAV," *Sensors*, vol. 21, no. 4, pp. 1224, Feb. 2021. Article (CrossRef Link)

[26] X. Chen, X. Huang, and D. Zhu, et al., "Research on chaotic flying sparrow search algorithm," *Journal of Physics: Conference Series*, vol. 1848, no. 1, pp. 012044, Jan. 2021.
Article (CrossRef Link)

[27] Z. Zhang, R. He, K. Yang, "A bioinspired path planning approach for mobile robots based on improved sparrow search algorithm," *Adv. Manuf.*, vol. 10, pp. 114–130, Aug. 2022.
Article (CrossRef Link)

[28] X. Li, X. Ma, F. Xiao, et al., "Time-series production forecasting method based on the integration of Bidirectional Gated Recurrent Unit (Bi-GRU) network and Sparrow Search Algorithm (SSA)," *Journal of Petroleum Science and Engineering*, vol. 208, pp. 109309, Jan. 2022.
Article (CrossRef Link)

[29] P. Kathiroli, K. Selvadurai, "Energy efficient cluster head selection using improved Sparrow Search Algorithm in Wireless Sensor Networks," *Journal of King Saud University-Computer and Information Sciences*, vol. 34, no. 10, pp. 8564-8575, Nov. 2022. Article (CrossRef Link)

[30] A. Tutueva, E. Nepomuceno, A. Karimov, et al., "Adaptive chaotic maps and their application to pseudo-random numbers generation," *Chaos, Solitons and Fractals*, vol. 133, pp. 109615, Apr. 2020. Article (CrossRef Link)

[31] R. Barros, J. Hidalgo, D. Lima Cabral, "Wilcoxon rank sum test drift detector," *Neurocomputing*, vol. 275, pp. 1954-1963, Jan. 2018. Article (CrossRef Link)

Mengfei Wang is a Ph.D. student at Chang'an University with a focus on Intelligent Transportation and Information System Engineering. Her primary research interests are digital image processing, artificial intelligence, and optimization algorithms.

Weixing Wang is a professor at the School of Computer Science, Chang'an University. His main research directions are image processing and computer vision.

Sheng Feng is an associate professor with the Department of Computer Science and Engineering, Shaoxing University. His research interests are in the area of intelligent robot, computer vision and wireless sensor networks.

Limin Li is an associate professor at the School of Electrical and Electronic Engineering, Wenzhou University. His main research directions are signal detection and image processing.